

Supplementary Information

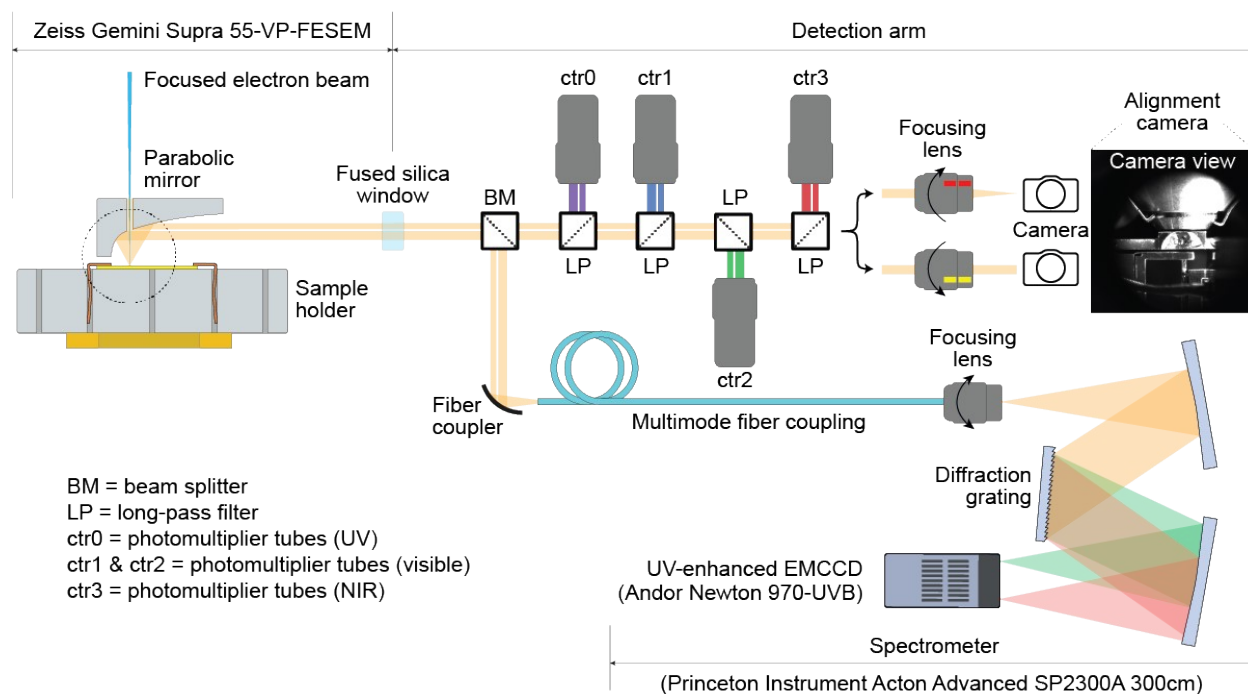
Optimizing cathodoluminescence microscopy of buried interfaces through nanoscale heterostructure design

Luca Francaviglia^a, Jonas Zipfel^a, Johan Carlstroem^a, Sriram Sridhar^{a,b}, Fabrizio Riminucci^{a,c}, Daria Blach^{a,d}, Ed Wong^a, Edward Barnard^a, Kenji Watanabe^d, Takashi Taniguchi^d, Alexander Weber-Bargioni^a, David F. Ogletree^a, Shaul Aloni^a, Archana Raja^{*a}

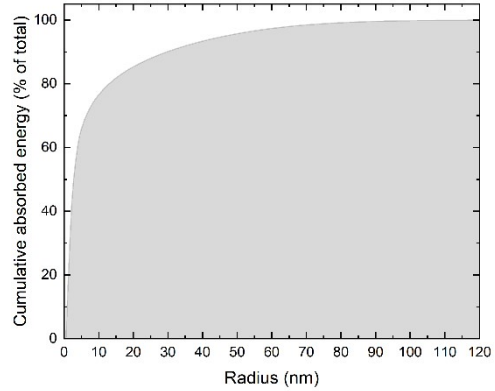
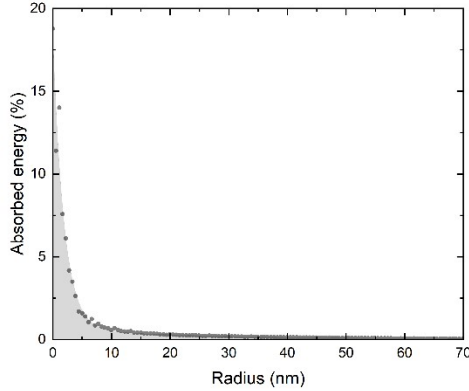
- Molecular Foundry, Lawrence Berkeley National Laboratory, 1 Cyclotron Rd., Berkeley, CA, USA
- Department of Materials Science and Engineering, University of California, Berkeley, CA 94720, USA
- Dipartimento di Fisica, Università del Salento, Strada Provinciale Lecce-Monteroni, Campus Ecotekne, Lecce, 73100, Italy
- Department of Chemistry, Purdue University, West Lafayette, IN 47909, USA
- National Institute for Materials Science, Namiki 1-1, Tsukuba, Ibaraki 305-0044, Japan

*Corresponding author: araja@lbl.gov

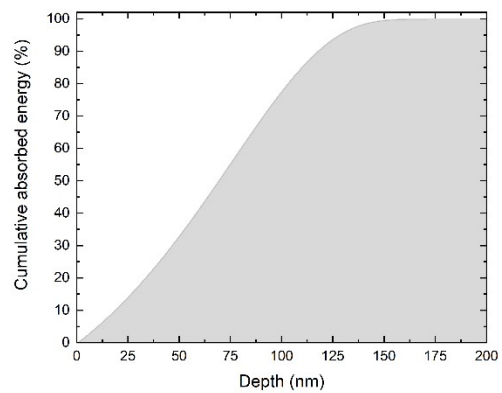
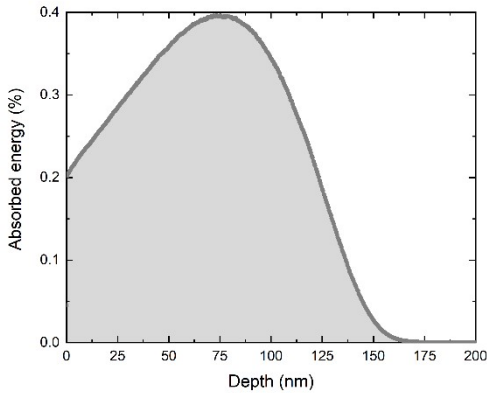
S1 CL setup diagram



S2 Absorbed energy spatial profiles

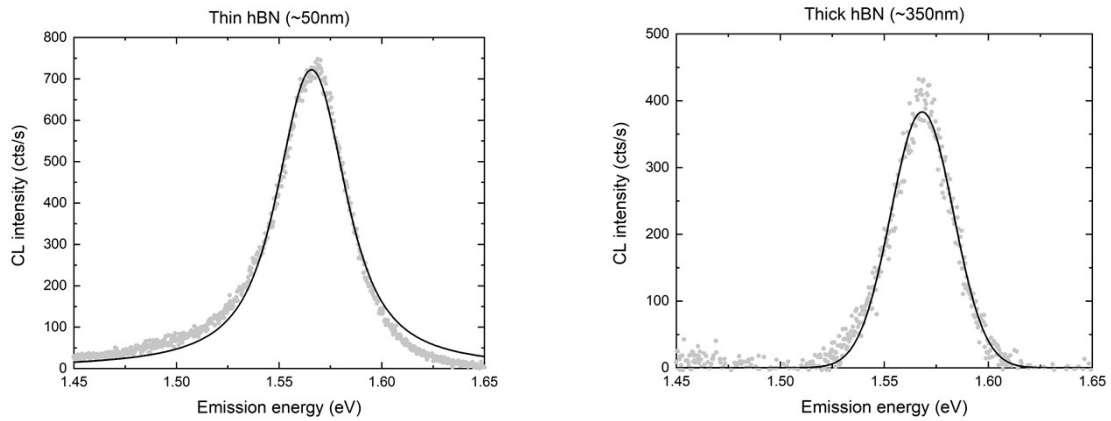


Radial profile of the electron interaction volume (CASINO MonteCarlo simulation of 1 million electrons) for an initial gaussian beam of 5 nm radius and 3 kV acceleration, when free to scatter until they release all their energy into infinitely thick (bulk) hBN. Gray dots are data points from the simulation, the gray shade is a guide to the eye following a double exponential fit of the data points.

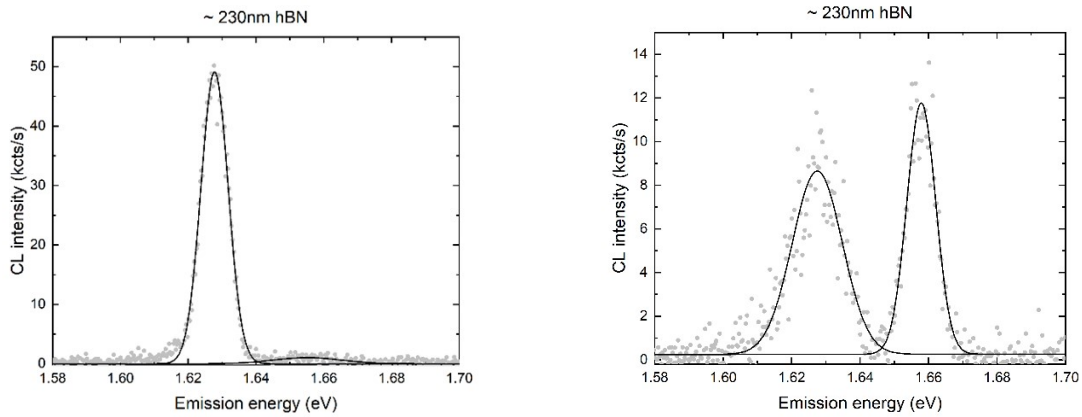


The CL brightness is proportional to the amount of energy that transfers into hBN from the interaction volume. Neglecting light interference, CASINO simulations (1 million simulated electrons at initial acceleration of 3kV) shows the proportion of CL brightness vs depth in hBN (left) and relative integral (right).

S3 CL spectra



RT MoSe2 CL spectra through thin and thick hBN (same peak position = 1.568eV, thick hBN FWHM slightly thinner than the thin one, 35meV vs 40meV).



20K MoSe2 CL spectra through 230nm hBN (peak positions: right, 1.628eV with FWHM 9meV and 1.655eV with FWHM 24meV; left, 1.628eV with FWHM 17meV and 1.658eV with FWHM 10meV).

S4 PL and CL spectral fit from figure 2a in the main manuscript

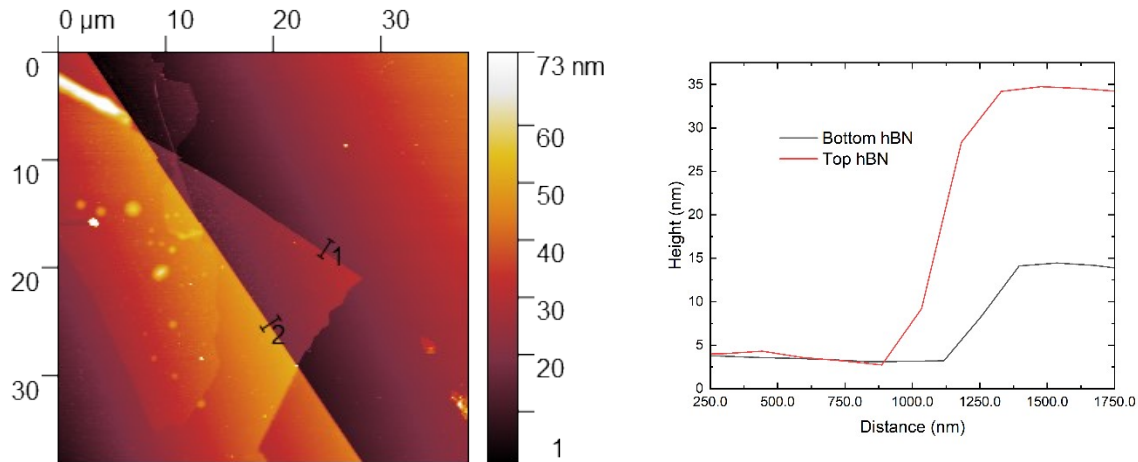
PL peak fit: hBN 54+/-5nm, grating 300l/mm, sample 20-07-14-A

Peak Type	Center Max (eV)	Max Height (cts)	FWHM (eV)
Gaussian	1.625	116	0.020
Gaussian	1.630	181	0.007
Gaussian	1.657	31	0.017

CL peak fit: hBN 263+/-9nm, grating 300l/mm, sample 21-06-25-A

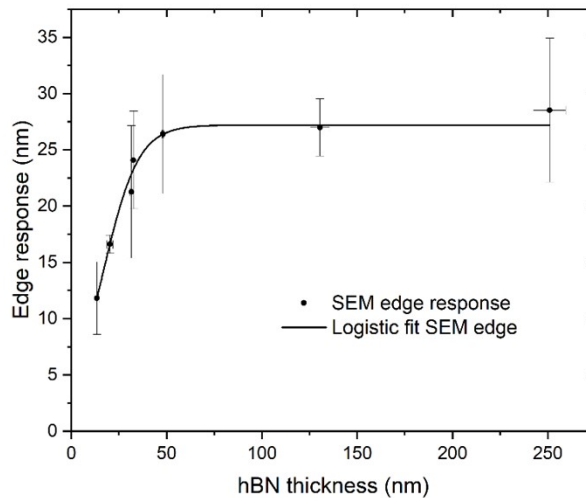
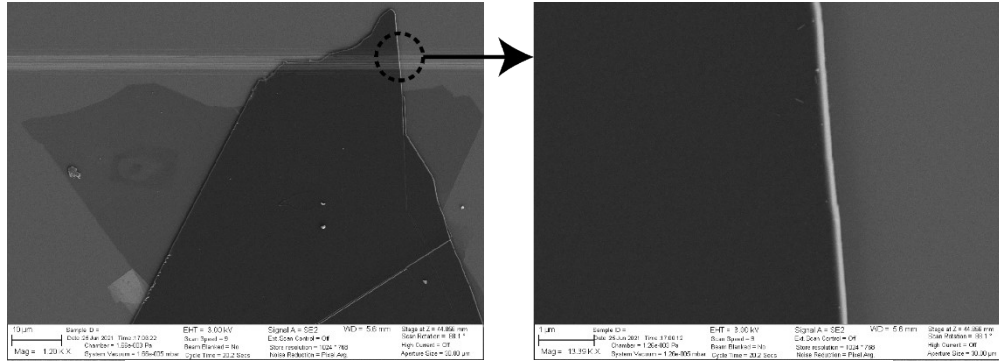
Peak Type	Center Max (eV)	Max Height (cts)	FWHM (eV)
Gaussian	1.621	164	0.022
Gaussian	1.629	834	0.012
Gaussian	1.657	288	0.010

S5 AFM of hBN layers



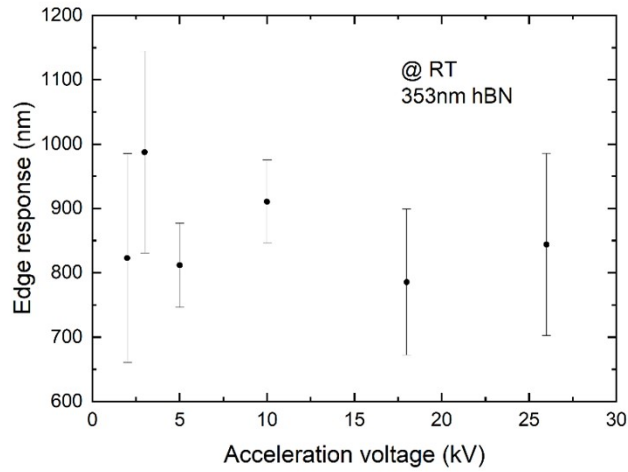
Left: AFM of flake edge in figure 1b main manuscript. Right: height profiles along lines 1 (thinner bottom hBN) and 2 (thicker top hBN) in the AFM map. For each sample, we measured a few profiles and reported the average in the main manuscript with the standard deviation of the measurements as uncertainty. The sample shown here has an average height of 43+/-2nm.

S6 SEM edge response

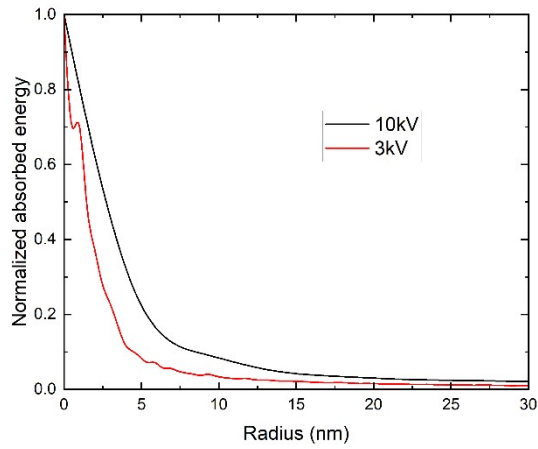


The top shows a typical SEM image of the free edges of two overlapped hBN flakes (top and bottom of a hBN-MoSe₂-hBN structure). The figure on the right zooms into a sharp edge of a 350nm-thick layer: we looked for sharp edges to measure the edge response of the SEM (only secondary electron imaging without CL signal). It is important to find sharp edges because hBN flakes of increasing thickness can show a terraced edge profile. For this reason, we selected hBN flakes that are not always those used in the manuscript. Similarly to figure 1, we measured the thickness of several hBN flakes by AFM and fitted linescans across the physical edges of the SEM images of these flakes. We took all measurements in the same conditions used in the main manuscript, in particular at 3 kV with a current of about 197pA. We report the average edge responses as a function of the hBN thickness. The standard deviations of the thickness and edge response data sets are the horizontal and vertical error bars, respectively. The SEM edge responses depend on both the microscope response and the physical interaction between the e-beam and the sample (spot size and size of the interaction volume in hBN). We fitted the data points with a logistic function and used this function to calculate the purely SEM edge response. The SEM edge responses start at about 10nm, increase almost nearly for very thin hBN and saturate around 50 nm to a constant value a bit below 30 nm. This trend reflects the increase in size of the interaction volume allowed in hBN flakes of increasing thickness up to a value for which the whole interaction volume is fully included in hBN.

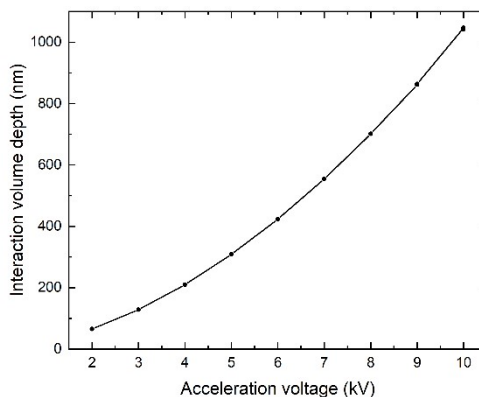
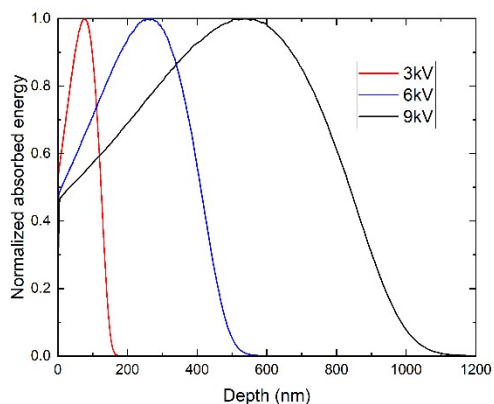
S7 Effect of acceleration voltage



Experimental edge response as a function of the acceleration voltage in the sample with 353 nm of total hBN thickness. Within the error bars, the edge response is constant. This observation corroborates the fact that the CL spatial resolution mainly depends on charge-carrier diffusion, while the size of the electron interaction volume has a negligible contribution.

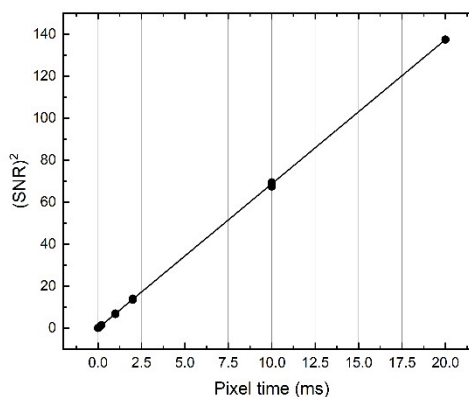
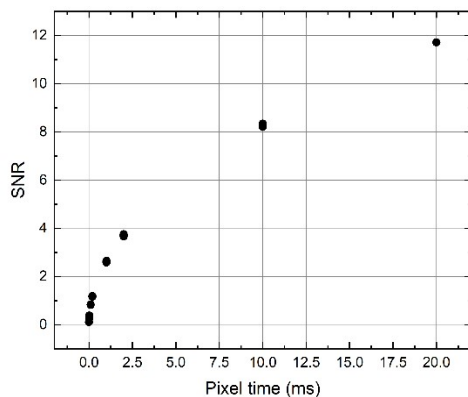


Simulations (performed under the same conditions as in S2) of the absorbed energy as a function of the lateral distance from the e-beam. The curves at different voltages are normalized to their maximum for comparison. Only a small difference in width is visible between the simulation at 3 kV and 10 kV.



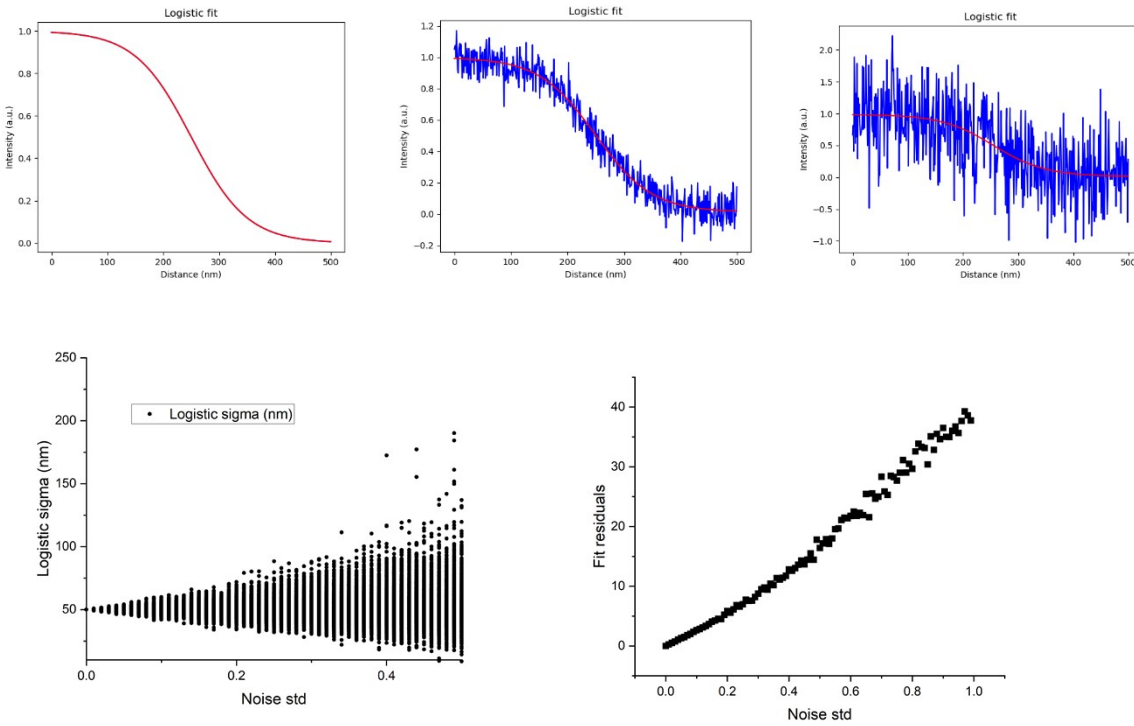
Left: simulations (performed under the same conditions as in S2) of the absorbed energy as a function of the depth in hBN. All curves are normalized to their maximum for comparison. The curves considerably change at different voltages, showing that more energy dissipates deeper in hBN with increasing voltage. Right: depth of the interaction volume (95% of total energy absorbed) as a function of the acceleration voltage. With increasing voltage, a significantly thicker hBN layer is necessary to absorb the total of the incident power.

S8 Experimental detector signal-to-noise ratio (SNR)



The SNR at PMT3 (used for the detection of the TMD signal) follows a clear square root function vs acquisition time, meaning that the main noise source is shot noise, with negligible contribution from the detector dark counts. This experimental observation supports the use of the RMS to simulate the noise in evaluation of the fit quality vs noise here below. The squared SNR shows an excellent linear increase as a function of time, with Pearson's $r = 0.99996$ and adjusted R-square 0.99991 .

S9 Fit quality vs noise



Edge response vs simulated white noise on ideal and known edge response function. Top: three noise levels on ideal curve (noise std 0, 8, and 45% of curve max). Left is increased uncertainty of edge response as sigma in logistic fit, right is increase in residuals. Linescans are usually taken with sufficient SNR but the SNR varies across different linescans collected. However, noise does not bias the edge response value in any specific direction (e.g. thicker hBN makes TMD brighter and less noisy does not systematically broaden or shrink the resolution).

S10 General factors affecting CL brightness

Together with the spatial resolution, also the signal intensity is another fundamental aspect of practical use that we can control through the sample design. The CL intensity I_{CL} is defined by the number of photons detected by the CL system over time. We can adapt the expression of the CL intensity [Cathodoluminescence microscopy of inorganic solids, B. G. Yacobi and D. B. Holt, Springer, 1990] to the case of TMD CL and write it as follows: $I_{CL} = f_D f_C f_A f_R \eta G$.

The factor f_D is a constant that accounts for the detection efficiency of the CL microscope; f_C accounts for the fraction of e-h pairs transfer from hBN to the TMD; f_A and f_R are factors that account for absorption and reflection losses, respectively; η is the radiative recombination efficiency of the studied emitter, which accounts for the fact that only a fraction of the MoSe2 excitons recombine in a radiative way; G is the fluence of hBN e-h pairs generated by the e-beam, thus expressed in the unit of time and volume.

The radiative recombination rate η depends on the intrinsic properties of MoSe2, while f_D depends on the specifications of the CL microscope. Therefore, both f_D and η are not under control by sample design and we did not consider them in the manuscript. A detailed understanding of f_C involves a variety of phenomena that limit the number of hBN e-h pairs that relax on the TMD energy levels and is beyond the scope of this discussion; these phenomena include the efficiency of charge transfer at the hBN-MoSe2 interface, the trapping of charge carriers on spatially localized hBN states, and the recombination of e-h pairs in hBN before reaching the TMD. The latter is the only aspect that we can tune by changing the hBN thickness: assuming a limited diffusion length of the e-h pairs in hBN, there is a value of hBN thickness for which charge carriers cannot reach the TMD. However, in the range of thickness values that we use here, we did not reach this condition (as already observed, the TMD CL brightness does not decrease in the thickest samples that we observed). Therefore, we neglected f_C in the following discussion.

Therefore, in the manuscript, we focus on the control of f_A , f_R , and G through the sample geometry.

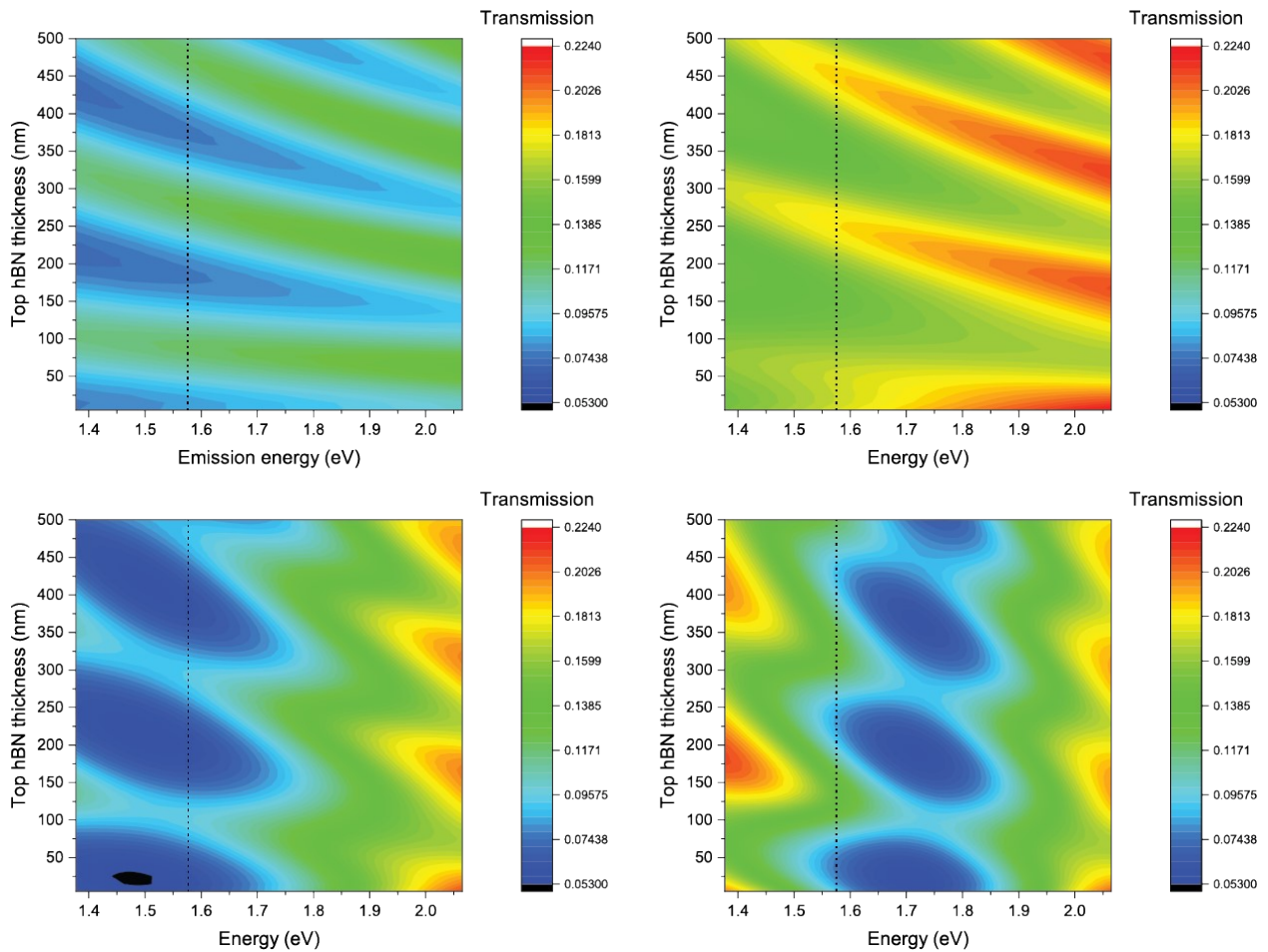
S11 Lumerical simulations

Lumerical (<http://www.lumerical.com>) is a commercial software that solves Maxwell's equations by an implementation of the finite-difference-time-domain method. The user can build the system geometry, composition, and optical properties. To simulate the hBN-encapsulated MoSe2 monolayers, we placed an emitting dipole in between two layers of hBN, with the dipole axis lying parallel to the hBN surfaces. This configuration mimics bright excitons in real TMD MLs, where light emission is collected from excitons oscillating in the TMD plane and emitting perpendicularly to the TMD surface. The bottom hBN layer of the hBN-dipole-hBN sandwich is in contact with a 2nm layer of Silicon oxide (to simulate the native oxide in real wafers) on top of a Silicon substrate. We evaluated the transmission of the dipole emission through the top hBN layer by using a far-field projection of the emitted light and integrating the far-field distribution to obtain the whole transmitted power. Because of the presence of an inhomogeneous dispersive medium and the small mesh size used in the simulations, the total dipole power radiated must be calculated through a box composed of six frequency-domain surface monitors placed around the dipole. The result was then used to determine the radiated power in the far field [M. H. Chowdhury et al., *J. Phys. Chem. C* 2008, 112, 11236–11249 and M. Kuttge et al., *Nano Lett.* 2010, 10, 5, 1537–1541].

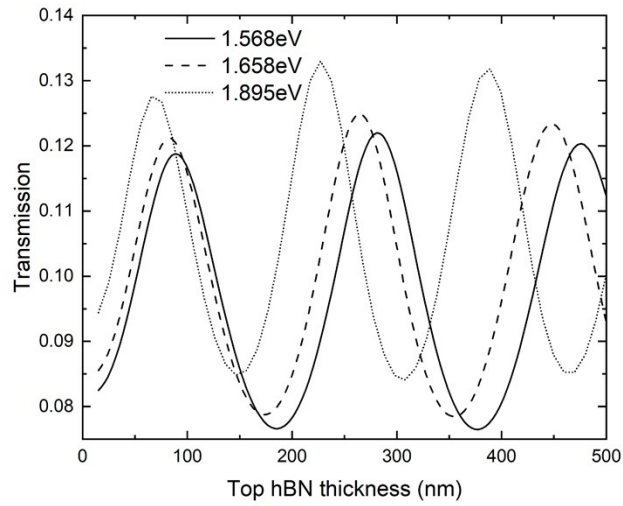
With the general structure and method described above, we were able to calculate the transmittance of the dipole emission for wavelengths between about 1.4 eV and 2eV: this energy range includes most of the TMD emission lines at room and low temperature. For a fixed thickness of the bottom hBN layer, we ran simulations with different thicknesses of top hBN to calculate the light transmission as a function of the top thickness. We chose four different values of the bottom hBN thickness (20 nm, 50 nm, 200 nm, and 350nm). For each of these values, we ran simulations with top hBN thicknesses from 10nm up to 500 nm.

We initially ran all simulations in two dimensions (2Ds) (following figure) to gain a qualitative understanding of the effect of hBN on the intensity of the transmitted light; we also checked the angular dispersion of the emitted light and confirmed that our experimental geometry allows the collection of most of the emitted light.

We then ran a simulation in three dimensions (3Ds) only for the case with 20nm of bottom hBN, which corresponds to the experimental conditions. With a 2D simulation, one cannot extrapolate the dipole source in the direction perpendicular to the simulated plane: a 2D simulation assumes that the system is invariant in the direction perpendicular to the simulated plane; this approximation corresponds to an infinite line source along that direction, which is different from an actual point dipole source: only a 3D structure can accurately simulate a point-like dipole. In fact, the 2D and 3D simulations give slightly different quantitative results, although they qualitatively match: the 2D simulation resulted in a higher transmission coefficient compared to the 3D one by two or three times.

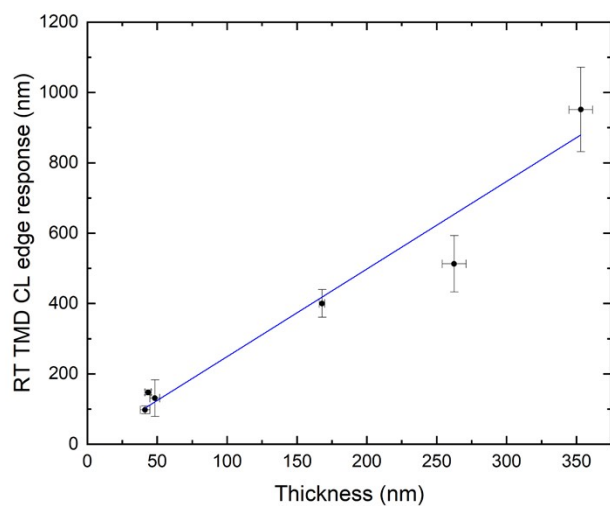


2D Lumerical simulation of light transmission from increasing top hBN thicknesses for different constant bottom hBN thicknesses (a) 20 nm, b) 50 nm, c) 200 nm, d) 350 nm). The dashed line is at 1.568eV, the MoSe₂ peak position at room temperature. The plots share the same colormap between 5.3% and 22.4%.



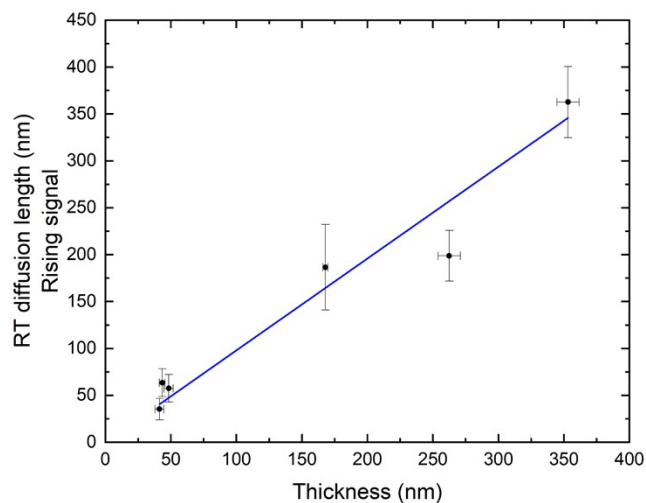
2D Lumerical simulations of light transmission at 1.568 eV, 1.658 eV, and 1.895 eV as a function of the top hBN thickness (constant 20 nm bottom hBN). The transmission maxima shift to thinner hBN with increasing light energy. At the two lowest energies, which include the range of the main MoSe₂ emission peaks at room temperature and 20 K, the first transmission maximum only slightly shifts from 89 nm to 83 nm of top hBN.

S12 CL edge response at room temperature



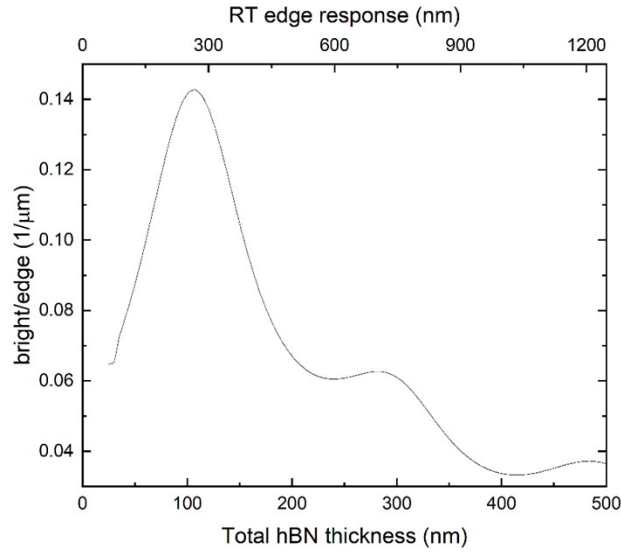
Edge response vs hBN thickness obtained like in the main manuscript, but at room temperature. The linear fit has a slope of 2.5nm +/- 0.1nm.

S13 Diffusion length at room temperature



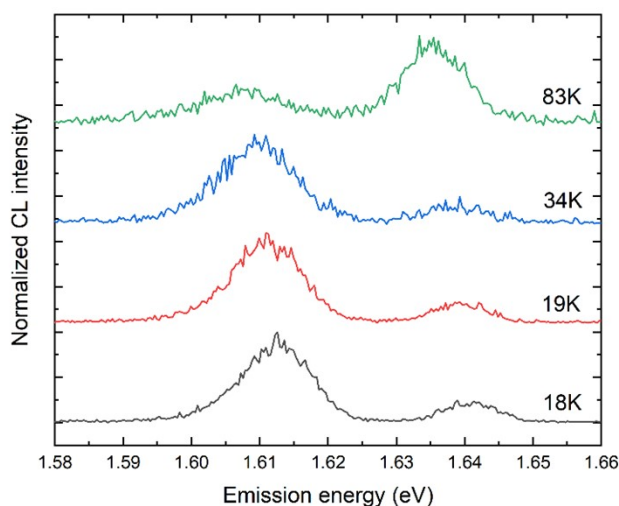
Effective room-temperature diffusion length as a function of hBN thickness (top and bottom layers). Linear-fit slope: 0.98nm +/- 0.06nm.

S14 Optimal working range at room temperature



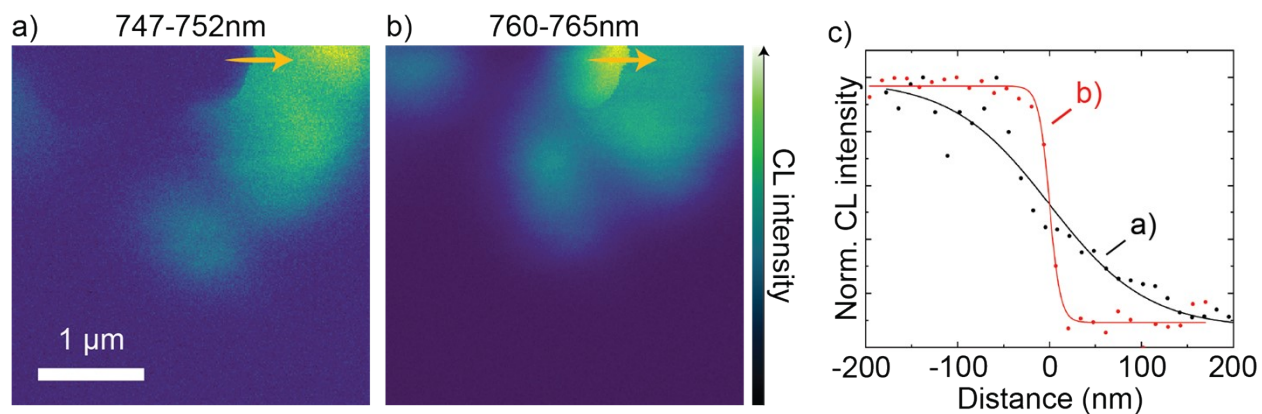
Relative CL brightness (deposited 3kV e-beam energy multiplied by the transmission coefficient) divided by the edge response at RT (photon energy of 1.568eV). We obtain this curve in the same way as the low-temperature equivalent shown in the main manuscript, but using all data from RT simulations (CASINO and 3D Lumerical) and RT experiments. We have no experimental data for thickness values beyond about 350nm, where the curve is a mere extrapolation. The curve shows a maximum at 107 nm, slightly thicker hBN than the low-temperature case. We can identify again an optimal working range for hBN thickness of 50-107nm.

S15 Temperature-dependent CL spectra



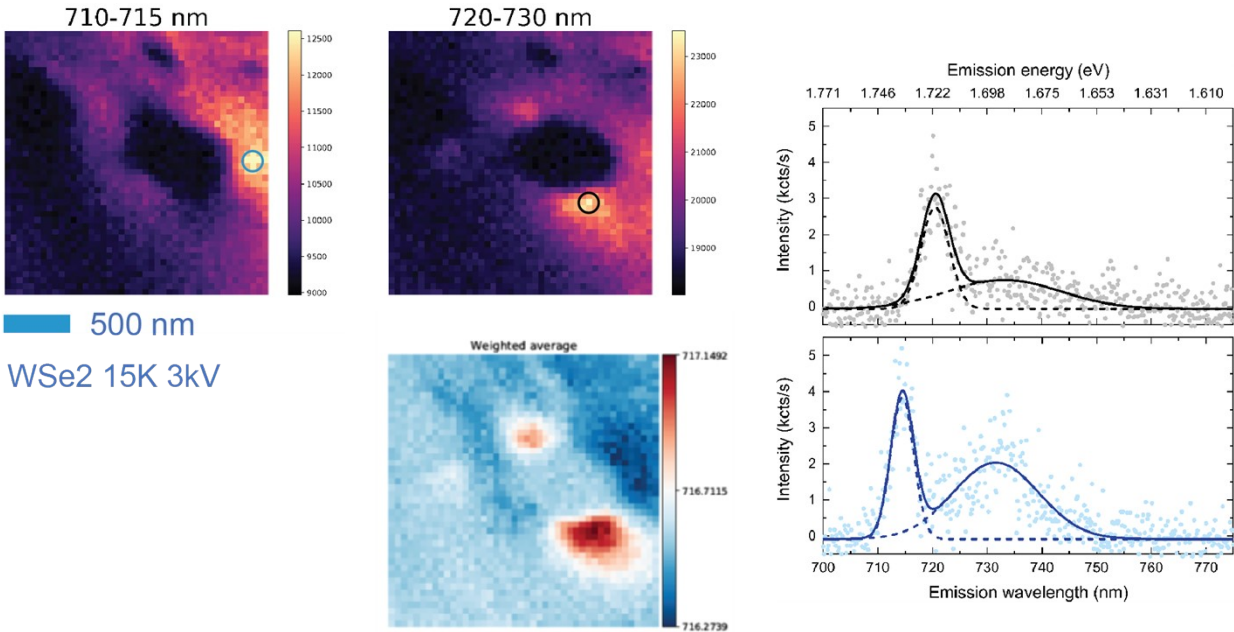
Single spectra acquired from the same area in the same MoSe₂ flake encapsulated in 353nm of total hBN. The low-energy peak becomes weaker at higher temperature, in favor of the high-energy peak. This behavior may further support the assignment of the low-energy peak to a charge exciton complex.

S16 Spectral filtering and spatial resolution



Hyperspectral CL map of a different region from the same sample as the one shown in figure 4. a) and b) are hyperspectral maps with energy selection in the wavelength interval indicated above them. They share the same scale bar of 1 μ m. c) reports the line scans along the yellow arrows in a) and b). The edge response from a) has a 10-90% width of 233nm \pm 31nm; the edge response from b) has a 10-90% width of 27nm \pm 4nm.

S17 WS₂ hyperspectral CL map at low temperature



Low-temperature hyperspectral maps of a WSe2 monolayer encapsulated in hBN. The black and blue spectra on the right are taken from a single pixel in the black and blue circles in the hyperspectral maps on the left. The map at the bottom shows the energy of the average weighted by intensity for each spectrum. These maps show that there is a clear redshift (about 14 meV) of the main peak in the positions along a direction that intersects the bubbles from the top left to the bottom right (red pixels in the bottom map). The redshifted peak also undergoes a slight broadening. In the other regions surrounding the bubble-like feature, this peak is in its original energy position but a more prominent low-energy broad peak appears.

Therefore, different phenomena are at the origin of the two behaviors. The redshift of the peak position may depend on the presence of anisotropic strain along the diagonal direction, possibly due to the bending of the TMD by the bubble. However, the bubble may also derive from the presence of polymer residues which may locally alter the dielectric environment of the TMD and shift its emission energy. On the contrary, the localized emission at low energy is more likely due to the presence of a point-like defect that favors the localization of a charge exciton complex.